ELSEVIER

Contents lists available at ScienceDirect

Materials Science & Engineering C

journal homepage: www.elsevier.com/locate/msec



Microfluidic-assisted polymer-protein assembly to fabricate homogeneous functionalnanoparticles



Libo Zhang^a, Andrew Beatty^a, Lin Lu^a, Akrm Abdalrahman^b, Thomas M. Makris^a, Guiren Wang^{b,*}, Oian Wang^{a,*}

- ^a Department of Chemistry and Biochemistry, University of South Carolina, 631 Sumter Street, Columbia, SC 29208, USA
- b Biomedical Engineering Program and Department of Mechanical Engineering, University of South Carolina, 300 Main Street, Columbia, SC 29208, USA

ARTICLE INFO

Keywords: Polymer protein co-assembly Homogeneous nanoparticle Microfluidics Electrokinetics Fast mixing

ABSTRACT

Functional polymer-protein nanoparticles (NPs) have broad applications in biotechnology and nanotechnology. In principle, controllable and vigorous mixing is required to fabricate homogeneous NPs, which remains a challenge via conventional bulk synthetic methods. In this study, an electrokinetics (EK) based microfluidic reactor with fast mixing is explored to assemble functional proteins with polymers in an ethanol/water cosolvent system. The resultant NPs show significantly improved size distribution by comparison with the ones prepared using conventional bulk method, while the NPs size can be tuned by adjusting the mass ratio of polymer to protein. The functionalities of the assembled proteins are sustained upon the EK based microfluidic mixing, indicating the application potential of our method in the controlled assembly of different functional proteins.

1. Introduction

Polymeric nanoparticles (PNPs), because of their small size, high surface-area-to-volume ratio, and easy tunable physical and chemical properties, have gained great attentions in materials science [1,2]. Through chemical modification of polymer chains [3] or conjugation with distinct functional molecules (e.g. inorganic or organic molecules, lipids, peptides, and proteins), [4-8] PNPs could be tailored with customized properties, and were found numerous applications in the fields of medicine, [9] bioimaging, [10] sensing [11,12] and catalysis [13,14]. Among them, the controlled assembly of polymers and/or proteins via supramolecular interactions offers unique opportunity in understanding the spontaneously self-organization process and fabrication of bioactive PNPs [15-21]. Currently PNPs are usually prepared using standard bulk reaction conditions, [22-26] which generally lead to large variability in their size distribution. In fact, it remains difficult to reproducibly synthesize batches of homogenous PNPs in bulk reactors, primarily due to the uncontrolled and insufficient mixing in addition to the uncontrolled residence time during the PNPs formation [27]. Therefore, methods that provide precise control of PNPs size distribution (for example, through microfluidics by optimizing mass transfer kinetics and diffusion rates, etc.) are of high interests [27-30].

In our previous work, we systematically studied the co-assembly of

poly(4-vinylpuridine) (P4VP) or other pyridine group grafted polymers with functional proteins to form core-shell PNPs [21,31-34]. The synthesis involved the mixing of polymer with protein in bulk reactors to form NPs intermediates, followed by dialysis or organic solvent evaporation for NPs maturation (Fig. 1a). The assembly is primarily controlled by a kinetic process driven by the reduction of interfacial tension, i.e., the polymer forms aggregates when experiencing nonsolvents. After this nucleation step, proteins, acting as a surfactant-like role, are absorbed on the surface to stabilize the NPs. We hypothesize the protein absorption is a relative slower step compared to the fast nucleation during the co-assembly. Both the fine balance between hydrophobicity and hydrophilicity as well as the hydrogen bonding between proteins and polymers are necessary for a successful co-assembly [21]. Nevertheless, because of the insufficient and less controllable mixing in bulk reactors, the polymer and polymer-protein particles experienced heterogeneous solvent environment during co-assembly, resulting in a broad size distribution of the NPs [21,31,33].

Using microfluidics based microreactor to synthesize various functional nanoparticles has attracted attentions because of its unique advantages, such as controllable transportation at microscale, significantly reduced diffusion distance, etc. [35] With improved diffusion process via geometrical design, microfluidics based mixers have been used for synthetic purposes [29,36,37]. However, because normally

E-mail addresses: guirenwang@sc.edu (G. Wang), wang263@mailbox.sc.edu (Q. Wang).

^{*} Corresponding authors.

Fig. 1. (a) Schematic illustration of proposed polymer-protein co-assembly process. (b) Schematic illustration of the entrance of microchannel which is used for polymer protein co-assembly. The fluids with different electrical conductivity (σ 1 & σ 2) in the non-parallel microchannel are driven by the hydrodynamic force f_h and the flow is excited by the electrical body force f_e which can be divided into x-components f_{ex} and y-component f_{ey} . f_{ex} at different points along the electric line can be either negative or positive related to f_h . The large force in x-direction ($f_h + f_{ex}$) and y-direction f_{ey} can generate a shear stress and produce a micro vertex [38], resulting in ultrafast mixing.

Reynolds number is low in microfluidic devices, the flow is laminar and the corresponding mixing is conducted only through a molecular diffusion process, and thus is relatively slow and poor. For this reason, we have recently developed a method to generate turbulent-like flows to create ultrafast mixing in microfluidic system under electrokinetics (EK) forcing, [38,39] which provides novel opportunities for flow control and manipulation in microfluidics. In particular, it was found that rapid mixing could be achieved on both large and small scales in the majority of the microchannel under AC electric field [38]. For example, with a 20 $V_{\text{p-p}}$ voltage and 2 $\mu L/\text{min}$ flow rate, 77% mixing can be reached within 5 milliseconds (ms), [40] which is much faster than other reported EK based micromixers [41,42]. Moreover, the mixing process could be easily controlled and fine-tuned by adjusting the AC electric fields (e.g. voltage, frequency, signal phase shift) and flow rates, [43] which will make it a superior technique than conventional geometry based micro mixers regarding to controllable mixing manipulation

Herein, for the first time, we report the usage of this EK based microfluidic method (Fig. 1b) to achieve polymer-protein co-assembly in order to fabricate homogeneous polymer-protein nanoparticles. Nanoparticle size is the result of two competing processes: drop breakage and coalescence after nucleation [44]. In our system, when protein stream and polymer dissolved ethanol stream meet in the microchannel, polymer droplets between the two phases of fluids will form at the initial stage and can then coalesce. The EK flow induced shear stress may breakup larger drops to generate smaller ones to increase interfacial area, and thus to enhance molecular mixing. The particle size distribution depends not only on the dispersive and continuous phase properties, the presence of surface-active agents, the type of surfactants, and the presence of electrolytes, but also on the overall flow velocity and concentration fields. Therefore, in this contribution, different proteins, flow rates and protein/polymer mass ratios were tested for the coassembly via fast mixing of micro fluids. We demonstrate that the polymer-protein NPs fabricated using our microfluidic method are highly uniform, the NPs size is tunable, and proteins' function is well retained. Because it is much easier to scale up by parallelization of multiple channels compared to the bulk method, this EK-based microfluidic method has unique advantages in its application for polymer protein co-assembly.

2. Theory

The principle of generating chaotic EK flow and mixing is given below to illustrate qualitatively how the mixing is enhanced. There is an initial large electrical force that can overcome viscous force to generate strong chaotic flows. The Navier-Stokes equation with EK force can be described as

$$\rho(\partial u/\partial t + u \cdot \nabla u) = \nabla p + \mu \nabla^2 u + F_e \tag{1}$$

$$F_{e} = \rho_{f} E - \frac{1}{2} (E \cdot E) \nabla \varepsilon + \frac{1}{2} \nabla \left[\rho E \cdot E \left(\frac{\partial \varepsilon}{\partial \rho} \right) T \right]$$
(2)

$$\rho_f = \nabla \bullet (\varepsilon E) = \nabla \varepsilon \bullet E + \varepsilon \nabla \bullet E \tag{3}$$

where ρ , u, p, μ are the fluid density, flow velocity, pressure and dynamic viscosity respectively; F_e is electrical body force, which consists of the Coulomb force (1st term), dielectric force (2nd term) and thermal expansion (3rd term) respectively in Eq. (2); E is electric field, ρ_f is the free volume charge density; ε and σ are the electric permittivity and conductivity of the electrolyte respectively, and T indicates temperature. For incompressible fluids, the third term can generally be ignored [45]. In addition, for a given fluid, ε mainly depends on T. On the one hand, as the two initial streams with different conductivity σ meet together, the interface between the two streams can be assumed to be frozen within a very short distance before the electrokinetic flow starts to develop. On the other hand, the bulk flow and the generated strong mixing will also transfer potential heat caused by Joule heating to downstream and to the good heat conductive metal walls. Therefore, T variation due to electrothermal effects could be insignificant. Thus ε is assumed to be uniform in the flow, $\partial \varepsilon/\partial t \approx 0$ and $\nabla \varepsilon \approx 0$. So the second term force in Eq. (2) is also negligible. Then we have

$$F_e = \rho_f E \tag{4}$$

The transport equation of ρ_f for a bipolar system is: [46].

$$\frac{\partial \rho_f}{\partial t} + u \cdot \nabla \rho_f + \nabla \cdot (\sigma E) = \left(\frac{D_+ - D_-}{m_+ + m_-}\right) \nabla^2 \sigma + \left(\frac{D_+ m_+ + D_- m_-}{m_+ + m_-}\right) \nabla^2 \rho_f$$
(5)

where σ is the conductivity of the fluid, m_+ and m_- and D_+ and D_- are the mobility and diffusivity of positive and negative charges respectively. Since in liquid, Schmidt number is usually very large, to simplify the process to illustrate the major physics, the diffusion term can be negligible. Because of the large conductivity different between the two streams, E will generate ρ_f near the interface, and the transport of ρ_f is primarily dominated by E, and thus, the convection u is relatively negligible. Then Eq. (5) can be simplified as:

$$\partial \rho_f / \partial t + \nabla \bullet (\sigma E) = 0 \tag{6}$$

Note although based on electro neutrality assumption, which is often adopted for transport phenomena in electrolyte, $\nabla \cdot (\sigma E) = 0$, such an approximation is not applicable here, not only because the well-known reasons described by Probstein, [47] but also because of the ρ_f created at the interface with a large difference in the conductivity between the two streams as shown in Fig. 1b. Near the interface, ρ_f should not be zero, as E has also a large difference at the interface between the initial two streams. The large difference in E is due to the difference in E0, which in turn generates E1 under local E2. Substitution of Eq. (3) into Eq. (6), yields:

(19)

$$\nabla \cdot E \approx -\left(\nabla \sigma \cdot E + \varepsilon \nabla \cdot \frac{\partial E}{\partial t}\right) / \sigma \tag{7}$$

Substituting Eq. (7) back into Eqs. (4) and (3), we find that the initial F_e can be approximately determined by:

$$F_{e} = -\varepsilon \frac{\nabla \sigma \cdot \mathbf{E}}{\sigma} E - \frac{\varepsilon^{2}}{\sigma} \left(\nabla \cdot \frac{\partial \mathbf{E}}{\partial t} \right) E \tag{8}$$

Here the first term of Eq. (8) is consistent with the result in DC case, [48] the second term is related to the initial F_e due to AC E. However, in practice, to satisfy quasi-electrostatic condition, normally

$$\varepsilon_{ref} \, \omega < \sigma_1 < \sigma_2 - \sigma_1 \tag{9}$$

where $\sigma 1$ and $\sigma 2$ are σ of the stream 1 and 2 respectively. Then the 2nd term of Eq. (8) should be much smaller than the 1st term and can be neglected. We have

$$F_{e} = -\varepsilon \frac{\nabla \sigma \cdot E}{\sigma} E \tag{10}$$

Eq. (10) indicates that F_e increases with increasing $\nabla \sigma$ and E_{\bullet} and parallelizing them. Initially, at a large scale where the influence of fluid viscosity is small, F_e directly drives and causes strong chaotic EK flow. The order of the corresponding velocity can be reached by balancing the inertial term and F_e in Eq. (1) as

$$U_e = \sqrt{\varepsilon_{ref}(\sigma_2 - \sigma_1)E_0^2/\rho\sigma_1}$$
 (11)

At a specific length scale l, where the time scale of convection under forcing $(\tau_e = l/U_e)$ is equal to the corresponding viscous diffusion time scale $(\tau_d = \rho l^2/\mu)$, a nominal length scale in the EK flow can be qualitatively concluded:

$$l_{ed} = \sqrt{\mu^2 \sigma_1 / \rho \varepsilon_{ref} E_0^2 (\sigma_2 - \sigma_1)} = \sqrt{w^2 / Gr_e}$$
(12)

$$Gr_e = (U_c l/\nu)^2 = \rho \varepsilon_{ref} w^2 E_0^2 (\sigma_2 - \sigma_1)/\sigma_1 \mu^2$$
 (13)

where Gr_e is the nominal electric Grashof number. To describe the electrical conductivity field in Eq. (10), we need transport equation for conductivity. For a bipolar system uniform ε , if there are neither production nor consumption of charges, the transport equation for conductivity is: (Melcher 1981, page 5.33) [46].

$$\frac{\partial \sigma}{\partial t} + u \cdot \nabla \sigma$$

$$= -E \nabla [(m_{+} - m_{-})\sigma + m_{+}m_{-}\rho_{f}] - [(m_{-} m_{-})\sigma + m_{+}m_{-}\rho_{f}] \frac{\rho_{f}}{\varepsilon} + D_{e}$$

$$\nabla^{2}\sigma + \frac{m_{+}m_{-}}{m_{+} + m_{-}}(D_{+} - D_{-})\nabla^{2}\rho_{f}$$
(14)

$$D_e = \frac{D_+ m_+ + D_- m_-}{m_+ + m_-} \tag{15}$$

where D_e is an effective diffusivity. The concentration of the protein and polymer is important for the nanoparticle synthesis. The protein in the solution is charged, but the polymer is not. Ignoring the chemical reaction, the transport equation of their concentration can be described as (Truskey et al. page 362): [49].

$$\frac{\partial c_i}{\partial t} + u \cdot \nabla c_i = D_{mi} \nabla^2 c_i \tag{16}$$

$$D_{mi} = \frac{(z_{+} - z_{-})D_{+}D_{-}}{(z_{+}D_{+} - z_{-}D_{-})}$$
(17)

where c_i is concentration of each component i, i.e. either polymer or protein, z_{-} and z_{+} are the charge valance of protein and ions. For polymer D_{mi} is its own diffusivity, but for protein, D_{mi} is given in Eq. (17), where ions in buffer balance the charge of the protein. Let $u = U_c \hat{u}, t = \tau \hat{t}, x = U_c \tau \hat{x}, \nabla = \hat{\nabla}/U_c \tau, \sigma = \sigma_0 \hat{\sigma}, E = E_0 \hat{E}, p = \rho U_c^2, \varepsilon = \varepsilon_{ref} \hat{\varepsilon},$ $c = c_0 \hat{c}$, $\rho_f = \varepsilon E_0 \widehat{\rho_f} / U_c \tau$, we get the dimensionless form of Eqs. (1), (15) and (16) as

$$\left(\frac{\partial \widehat{u}}{\partial \widehat{t}} + \widehat{u} \cdot \widehat{\nabla} \widehat{u}\right) + \widehat{\nabla} \widehat{p} + \frac{(\widehat{\nabla} \widehat{\sigma} \cdot \widehat{E})}{\widehat{\sigma}} \widehat{E} = \frac{1}{\sqrt{Gr_e}} \widehat{\nabla}^2 \widehat{u}$$
(18)

$$\frac{\partial \widehat{\sigma}}{\partial \widehat{t}} + \widehat{u} \cdot \widehat{\nabla} \widehat{\sigma}$$

$$= \frac{R_{e,mig}}{\sqrt{Gr_e}} \left(\frac{m_+ - m_-}{m_+ + m_-} \right) (\widehat{E} \cdot \widehat{\nabla} \widehat{\sigma} + \widehat{\sigma} \widehat{\rho_f}) + \frac{\tau_r R_{e,mig}^2}{\tau_d \sqrt{Gr_e}} \left(\frac{m_+ m_-}{(m_+ + m_-)^2} \right) (\widehat{E}$$

$$\cdot \widehat{\nabla} \widehat{\rho_f} + \widehat{\rho_f}^2) + \frac{1}{Sc_e \sqrt{Gr_e}} \widehat{\nabla}^2 \widehat{\sigma} + \frac{\tau_r R_{e,mig}}{\tau_D \sqrt{Gr_e}} \left(\frac{m_+ m_-}{(m_+ + m_-)^2} \right) \widehat{\nabla}^2 \widehat{\rho_f}$$
(19)

$$\frac{\partial \widehat{c_i}}{\partial \widehat{t}} + \widehat{u} \cdot \widehat{\nabla} \widehat{c_i} = \frac{1}{Sc_{mi} \sqrt{Gr_e}} \widehat{\nabla}^2 \widehat{c_i}$$
(20)

where \hat{u} , $\hat{\nabla}$ and \hat{E} , $\hat{\sigma}$, and $\hat{\rho_f}$ are dimensionless functions of u, x, ∇ ,E, σ and ρ_f respectively; $\sigma_0 = \sigma_2 - \sigma_1$ is the initial characteristic σ of the flow; $E_0 = V_f / \sqrt{2} w$ represents the nominal E across the channel width w(where V_f is the applied peak-to-peak voltage between two electrodes. wis the width of the channel at the entrance.). $\varepsilon_{\textit{ref}}$ is the ε of water at a reference T; $Sc_e = \mu/\rho D_e$ and $Sc_{mi} = \mu/\rho D_{mi}$ are Schmidt number of effective ions and component i respectively; $\tau_{\rm r} = \epsilon/\sigma_0$ is charge relaxation time, $R_{\rm e,\ mig}=lE_0(m_++m_-)/v$ is charge migration Reynolds number, and $\tau_D=l^2/(D_+-D_-)$ is a charge diffusion time respec-

If Gr_e is sufficiently high, e.g. by increasing initial $(\sigma_2 - \sigma_1)$, the diffusion terms of the right side in Eqs. (18), (19) and (20) become approximately negligible. Both conductivity and concentration will be dispersed by U_e and chaotic EK flow without smearing in the entire transverse direction. This can even enhance F_e and thus, mixing at small scale to generate homogeneous c_i . By increasing the initial σ_2/σ_1 , E_0 and parallelizing $\nabla \sigma$ and E, Gr_e can be enhanced.

3. Experimental details

3.1. Microchannel fabrication

The design and fabrication of the microchannel is shown in Fig. S1 in supporting information. A quasi T-shaped microchannel was made of acrylic plates, gold chips, Teflon™ PFA membrane, Teflon™ PTFE sheets and gasket by lamination-based microfabrication [38]. Gold chips were used as electrodes to make the two electrically conductive channel sidewalls. Teflon™ PFA membranes were used to avoid the channel clogging problems caused by the high stickiness of polymer, which has been one of the major obstacles in microfluidic nanomaterials synthesis [50]. A Teflon™ PTFE splitter plate was used to separate the two steams initially till they meet in the microchannel and lead to a sharp interface with high conductivity gradient between the two streams, which can further enhance the mixing efficiency. The microchannel has a rectangular cross-section of 150 µm in width at the entrance and 230 µm in height, with the length of 5 mm. A small divergent angle of 5° was designed to maximize the mixing efficiency (Figs. 1b, S1) [38]. Rubbers were used to seal the channel. Because of the rapid polymer protein coassembly process under the ultrafast mixing, no significant polymer aggregates or other clotting issues were observed during the NPs fabrication with our microfluidic channel.

3.2. Materials

Teflon™ PFA membrane, Teflon™ PTFE sheets were purchased from Cshyde. Gold chips were purchased from Surepure Chemetals. Fluorescein sodium salt, P4VP (Mw 60,000), p-aminophenol (pAP, > 99.0%) were purchased from Sigma-Aldrich. Phenazine methosulfate (PMS, > 98.0%) was purchased from TCI America. NADH sodium salt was purchased from EMD Millipore. Unless otherwise noted, all chemicals and solvents used were of analytical grade and were used as received from commercial sources. Water (18.2 M Ω) was obtained from Milli-Q system (Millipore). The proteins used in this work include bovine serum albumin (BSA) (MW: 66 kDa, pI: 4.7), fluorescent protein EGFP (MW: 27 kDa, pI:5.6), fluorescent protein mCherry (Mw: 29 kDa, pI: 5.6), and N-oxygenase CmlI (Mw: 38 kDa, pI: 5.0). BSA was purchased from Sigma-Aldrich. All other proteins were expressed in *E. coli* BL21 (DE3) in LB medium, and purified by nickel-nitriloacetic acid (Ni-NTA) affinity chromatography as described previously [51,52]. PBS buffer (NaCl 137 mM, KCl 2.7 mM, Na₂HPO₄ 10 mM, KH₂PO₄ 1.8 mM, pH 7.4) was used unless otherwise noted.

3.3. Flow visualization

The microchannel was placed on an inverted fluorescent microscope (Olympus-IX70). Solution injection was done by a syringe pump (Harvard, Model PHD2000 Programmable) with different flow rates. AC electric power was supplied by a function generator (Tektronix, Model AFG3102). The visualization of the mixing process was conducted by Epi-fluorescence imaging technique.

3.4. Polymer-protein co-assembly

For P4VP protein(s) co-assembly with microfluidic method, P4VP dissolved in ethanol and protein(s) dissolved in PBS were injected by two different sizes of syringes (1 mL vs 10 mL). The syringe pump was used to control flow rates. AC electric power was supplied by the function generator to provide electric field. 20 $V_{p\text{-}p}$ voltage, 20 kHz frequency, 180° phase shift were used unless otherwise noted. For P4VP-protein(s) co-assembly with conventional bulk method, 100 μL of P4VP dissolved in ethanol was added into a glass vial containing 1 mL protein(s) dissolved in PBS buffer drop wisely during vigorous magnetic stirring. The concentration of P4VP and proteins solution was adjusted as the same among different methods. More than three batches of assembled samples were collected under each condition for characterization unless otherwise noted.

3.5. Polymer-protein NPs characterization

The hydrodynamic size distribution of nanoparticles was measured by Zetasizer (Nano ZS, Malvern Instruments). The mean value for the size based on the intensity, and the PDI, a dimensionless width parameter based on the cumulants analysis, were reported. For TEM analysis, the NPs samples were diluted 5 times by DI water, 20 μL diluted sample was dropped onto 250-mesh carbon-coated copper grids. The grids were dried, washed once by DI water and observed with a Hitachi H-8000 electron microscope. NPs size and size distribution based on TEM images were analyzed by ImageJ software.

For protein (BSA as a model) loading efficiency characterization, the NPs samples were centrifuged at 9 K rcf for 10 min at room temperature, the supernatants were collected for a standard Bradford assay. The loading efficiency on the NPs was calculated from the unbound proteins in the supernatant by subtracting the amount of the unbound proteins from the initial amount of proteins used.

For fluorescence imaging of polymer fluorescent protein(s) NPs, glass coverslips and plates were first soaked in a 10:1 (v:v) mixture of concentrated $\rm H_2SO_4$ and 30% $\rm H_2O_2$ overnight, extensively rinsed with water, sonicated in absolute ethanol for 10 mins and dried with air stream. The NPs samples after centrifuge were dispersed on the cleaned plates covered by a coverslip and sealed by nail polish oil. A self-assembled confocal microscope with an oil immersion, $60\times$ NA1.4 and PlanApo objective lens (Olympus). A continuous wave laser (477 nm, 100 μ W), filter cubes/sets and a photomultiplier tube (PMT, HAMAM-ATSU, R-928) were used.

CmlI catalyzed reactions with pAP were measured by monitoring pnitroso phenol (pNOP) product formation at an absorbance of 405 nm with a Molecular Device SPECTRAMax plus 384 with a microplate reader using 0.33 cm path length. Since CmlI enzyme is tolerant to ethanol [51], no ethanol evaporation or dialysis was done for P4VP- CmlI NPs sample. Instead, the assembled samples were used for activity test directly without purification. For different samples, the same amount of free enzyme and the same percentage of ethanol (9.1%) were used.

3.6. Conductivity and viscosity test

A conductivity meter (EXTECH ISTRUMENTS, ExStik II) was used for conductivity test. Viscosity was tested by Cannon-Ubbelohde Viscosity meter, #25.

4. Result and discussion

4.1. Mixing visualization

To demonstrate the EK-based fast mixing process, a modified quasi T-shaped microchannel was fabricated as shown in Fig. S1. Teflon materials were used to coat the inner faces of the microchannel in order to avoid the clotting problems. Firstly, fluorescein in PBS was mixed with deionized (DI) water using our microfluidic system. The conductivity ratio of these two streams was 5000:1. Different flow rates from 1 to 10 μ L/min were tested (Figs. 2a and b, S2 and Movies S1–S4 in the Supporting Information). In the absence of electric field, laminar flows were formed in the microchannel, and only some diffusion could be observed with slower flow rate (Fig. 2a). The boundary of the fluorescein solution and PBS solution was blurred with 1 μ L/min flow rate and became much clearer with higher flow rates ($\geq 2 \mu L/min$, Fig. S2a, S2c, S2e). While under electric field, chaotic flows were formed, which demonstrated dramatically enhanced mixing (Fig. 2b). Thus, significant increased diffusion is expected. A similar phenomenon was also observed with EGFP solution and polymer solution as injected as the two streams with ratio of \sim 6400: 1 (17,260 μ S/cm vs 2.7 μ S/cm) (Figs. 2c and d, S3 and Movies S5-S8). In Fig. 2c, since the flow rate of EGFP solution was much larger than that of the polymer solution, EGFP solution occupied the most space of the channel and the boundary moved to the polymer side significantly. The boundary was still visible, although it was less clear. In the absence of electric field, the laminar flow pattern depends on the Peclet number (Pe), which is determined by the flow rate for certain micro flows, and the ratio of the flow rate of the two streams [53]. The larger the Pe, the clearer the boundary of the two streams. For flow rates of 1 μ L/min (in Figs. 2a and c) or lower, the molecular diffusion in transverse direction becomes more important, and a less clear interface was seen. A clear boundary was observed when higher flow rates ($\geq 2 \mu L/min$) were used as shown in Figs. S2 and S3. Considering the much higher viscosity of P4VP polymer solution than that of DI water (2.1 mm²/s vs 1.0 mm²/s), we can conclude that the mixing under electric field is highly robust in this microfluidic channel. It is worthy to note that, with a 10 $\mu L/\text{min}$ flow rate, highly homogeneous mixture of EGFP solution and P4VP solution can also be achieved at around 150 μm downstream of the entrance under electric field (Fig. S3f), which implies a complete mixing starting from this position.

4.2. Improved size distribution of polymer-protein NPs via microfluidic method

Firstly, BSA was used as a model protein to fabricate P4VP-protein NPs in this microfluidic method. Proteins were dissolved in PBS buffer (0.05 $\mu g/\mu L$), and P4VP was dissolved in ethanol (0.5 $\mu g/\mu L$). Flow rates 2 $\mu L/min$ and 10 $\mu L/min$ were tested while the electric field condition was kept the same. Mass ratio of P4VP to BSA was fixed as 1:1 (the volume ratio $V_{P4VP}:V_{BSA}=10:1$). Dynamic light scattering (DLS) analysis shows that the hydrodynamic size distribution of NPs produced by microfluidics is significantly improved by comparing with the samples from conventional bulk method (Fig. 3). Transmission electron microscopy (TEM) images demonstrate highly homogeneous NPs

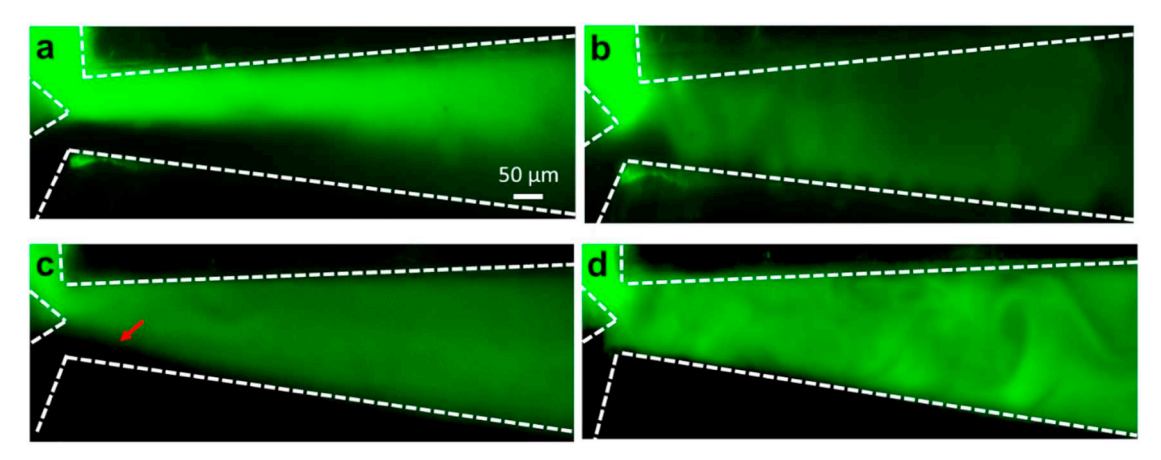


Fig. 2. Visualization of mixing process with fluorescein in PBS and DI water (a, b), EGFP protein in PBS and P4VP in ethanol (c, d) in the microchannel; (a, c) laminar flow without electric field. (b, d) chaotic flow with electric field. Flow rate was 1 μ L/min. For (a) and (b), two 1 mL syringes were used for fluorescein and DI water respectively. A 7 V_{p-p} voltage was used. For (c) and (d), 1 mL syringe was used for P4VP solution and 10 mL syringe was used for EGFP solution to maintain the low ethanol concentration in the final samples. A 20 V_{p-p} voltage was used. For all samples, 20 kHz frequency and 0.015 s exposure for imaging were used. The red arrow in (c) shows the small fractions of polymer solution and the interface of the two solutions in the channel. (For interpretation of the references to colour in this figure legend, the reader is referred to the web version of this article.)

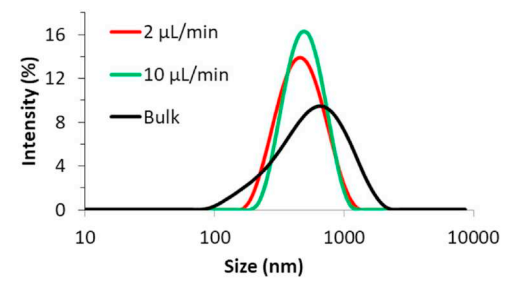


Fig. 3. DLS analysis of hydrodynamic size distribution of P4VP-BSA NPs fabricated by different methods. Final concertation of P4VP 0.05 mg/mL, BSA 0.05 mg/mL for all samples.

fabricated by microfluidic method (Figs. 4a–d, f–i), while the NPs from the conventional bulk method are less homogeneous in size (Fig. 4k–n). Size distribution of NPs at different areas of TEM grids was analyzed (Figs. 4e, j, o), which confirms significantly improved size distribution of NPs from microfluidic method. With higher flow rate, the polydispersity index (PDI) of NPs is slightly increased, likely due to the reduced mixing in the channel. On the other hand, if there was no electric field applied, much larger and inhomogeneous NPs (average size as 680 to 770 nm depending on flow rates) were produced, and

large amount of polymer aggregates could be observed under TEM (Fig. S4). Within the enhanced chaotic flows, proteins and polymer precursors can be well mixed in a very short time by increased shear stress. We postulate that during the co-assembly in micro flows under an AC electric field, the size of NPs and local concentration of the starting materials in the mixture can be balanced. Thus, continuous aggregation of unassembled polymers is suppressed. Additionally, the residence time distribution (RTD) of the assemblies is narrowed, which is ultimately responsible for the improved NPs' homogeneity.

4.3. The size of polymer-protein NPs is tunable

Our previous works showed that, driven by the interfacial energy, the surface composition and materials' concentration could influence the size of the P4VP-protein NPs [21,32]. When the mass ratios of polymer to protein were adjusted as 1:8, 1:0.8 and 1:0.08 for the two streams in the microchannel, different size of NPs were fabricated with 2 μ L/min flow rate. TEM images and DLS analysis show that the size of fabricated NPs increases with the increase of the polymer/protein mass ratio (Figs. 5a–d). The average hydrodynamic sizes are 284 nm, 523 nm and 925 nm with polymer/protein ratio as 1:0.8, 1:0.08 and 1:0.008, respectively. Again, by comparing with the NPs produced by conventional bulk method, the size distributions of NPs fabricated through

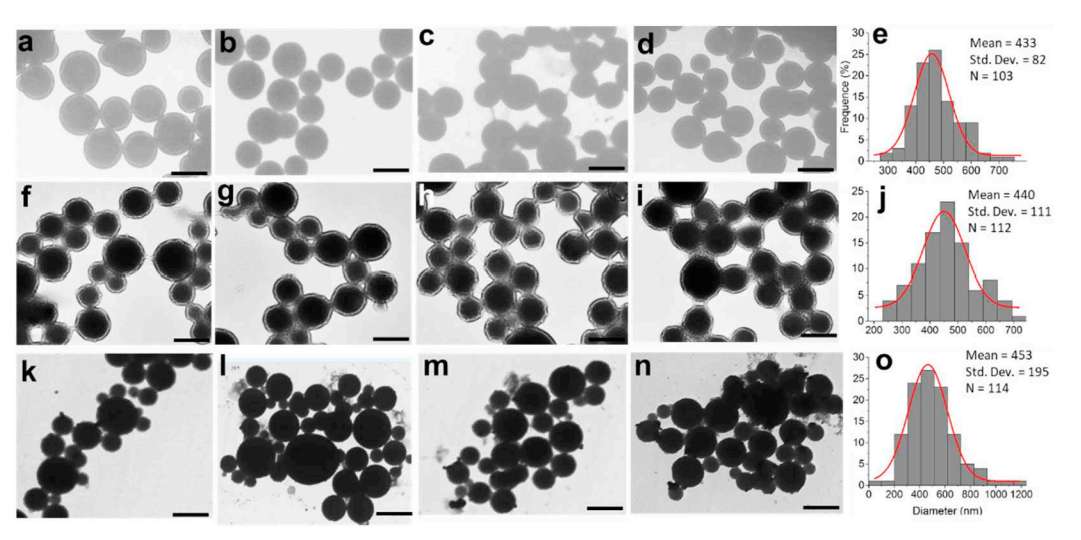


Fig. 4. Representative TEM images of P4VP-BSA nanoparticles fabricated by microfluidics with 2 μ L/min (a–d), 10 μ L/min (f–i) flow rates, and bulk method (k–n). Scale bars: 0.5 μ m. (e, j, o) Statistical analysis of the NPs size and distribution. The red curves are Gaussian fits to the corresponding histograms. For all samples, 0.05 mg/mL P4VP and 0.05 mg/mL BSA were used as final concentration. (For interpretation of the references to colour in this figure legend, the reader is referred to the web version of this article.)

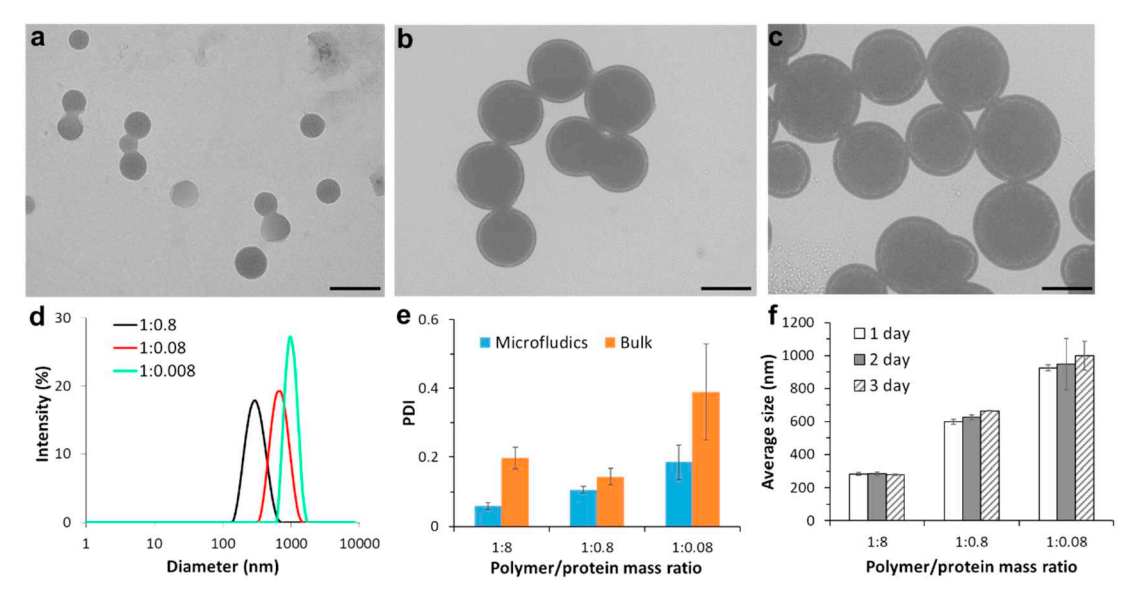


Fig. 5. Different size of P4VP-BSA NPs fabricated by adjusting polymer/protein ratio and the stability test. (a-c) Representative TEM images of P4VP-BSA with different size fabricated by microfluidics. Scale bars represent $0.5 \mu m$. (d) DLS analysis of different size of NPs fabricated by microfluidics. (e) PDI comparison of the NPs fabricated by microfluidics and conventional bulk method. **P-value < 0.01, *P-value < 0.05 by Student's *t*-test. (f) Average hydrodynamic size of NPs fabricated by microfluidics with different aging time at room temperature as detected by DLS. A fixed concentration of 0.05 mg/mL was used for P4VP, while BSA was adjusted from 0.4 mg/mL to 0.04 mg/mL to 0.004 mg/mL for the fabrication of small, medium, and large size NPs. Error bar stands for standard deviation of triplicate samples.

microfluidics were significantly improved (Figs. 5e and S5a-d). While the NPs fabricated by microfluidic method are stable at room temperature (Fig. 5f), the size of NPs prepared by conventional bulk method shows growth within 3 days' incubation at room temperature, especially when high polymer/protein ratio was used (Fig. S5e), we rationalize that it was caused by the agglomeration of polymers and NPs due to scattered protein coating on the surface of NPs [31,33]. The sustained size and morphology of NPs during the ethanol evaporation as well as long-term storage at 4 °C indicate that mature and stable polymer protein NPs have been formed via microfluidic co-assembly (Fig. S6). The interactions between polymer and proteins and the benign microenvironment provided by polymers likely contribute to the stability of the enzyme and the resultant assemblies. The protein loading efficiencies of NPs fabricated with the microfluidic method under different conditions (with 2 μ L/min to 10 μ L/min flow rates and 1:1 to 1:10 polymer/protein mass ratios) were measured (Fig. S7). They were around 70%, demonstrating a good protein loading capacity using this microfluidic method. Interestingly, if the entrance width of the microchannel is decreased into 90 µm, much smaller NPs can be fabricated, nevertheless the NPs size cannot be well-controlled by adjusting polymer/protein mass ratio anymore (Fig. S8). We believe that the matching of mixing time and co-assembly time is critical to control the size of final NPs. With further increasing mixing intensity, the NPs size could be insensitive to the starting materials ratio. Similar phenomenon has been reported for self-assembly of copolymeric NPs [54].

4.4. Polymer-fluorescent proteins co-assembly and function test

To characterize the structural change of NPs fabricated by microfluidic method, EGFP and another fluorescent protein mCherry (or BSA) were used to *co*-assemble with P4VP polymer to produce polymer multiprotein NPs P4VP-EGFP-mCherry and P4VP-EGFP-BSA. Mass ratio of polymer/EGFP/mCherry (or BSA) was fixed as 4:1:1. The BSA was used in the P4VP-EGFP-BSA to balance the polymer protein ratio to control the NPs size. TEM imaging reveals that the homogeneous polymer proteins NPs were fabricated successfully by microfluidic method (Figs. S9a–c). Fluorescence images of P4VP-EGFP-mCherry and P4VP-EGFP-BSA NPs were taken by a laser scanning confocal microscopy (Fig. 6).

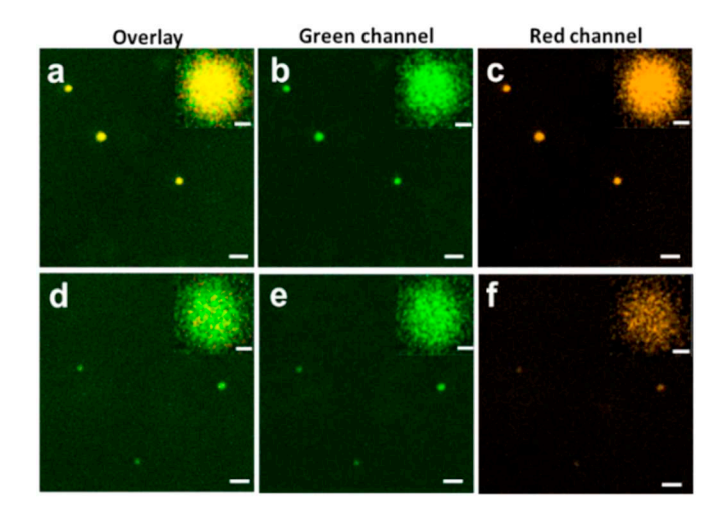
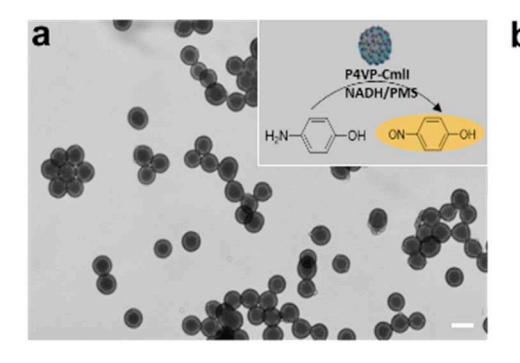


Fig. 6. Function characterization of P4VP-protein(s) NPs prepared by microfluidic method. Fluorescence microscopy images of P4VP-EGFP-mCherry (a–c), P4VP-EGFP-BSA (d-f) show the sustained fluorescence protein(s) function on NPs and a significant FRET effect (insets). 0.05 mg/mL P4VP, 0.0125 mg/mL EGFP, 0.0125 mg/mL mCherry or 0.0125 mg/mL BSA and 10 μ L/min flow rate were used for co-assembly. Scale bars: 5 μ m. Insets: representative image of single P4VP-EGFP-BSA and P4VP-EGFP-mCherry NP; Scale bars: 500 nm.

This laser is suitable to excite EGFP and minimize the 'cross talk' signal from mCherry simultaneously (P4VP-mCherry-BSA NPs cannot be detected, data not shown). Both P4VP-EGFP-mCherry and P4VP-EGFP-BSA NPs showed bright signal in green channel. By excluding the effect of EGFP 'leaking' signal in red channel and the minimal 'cross-talk' signal from mCherry, the red/green signal intensity ratio was calculated for P4VP-EGFP-mCherry and P4VP-EGFP-BSA single NPs to show an apparent fluorescence resonance energy transfer (FRET). The red/green signal intensity ratio of P4VP-EGFP-mCherry is much higher than that of P4VP-EGFP-BSA (~two-fold changes, Fig. S10), which reveals significant FRET occurring between the assembled EGFP and mCherry on the NPs. This result not only demonstrates the function of both fluorescent proteins still sustained but also implies a very closed distance



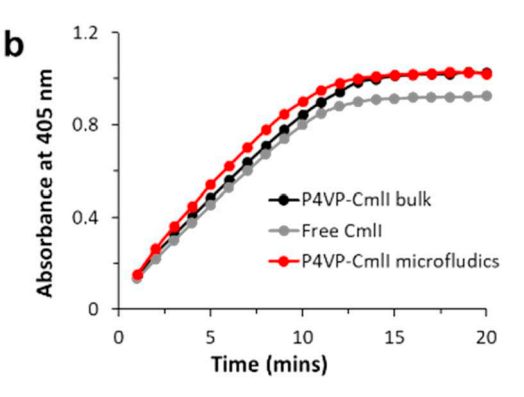


Fig. 7. (a) Representative TEM image of P4VP-CmlI NPs generated by microfluidic method and the chromogenic reaction scheme (inset), which can be used to characterize the polymer-enzyme NPs' activity. 2 μL/min flow rate was used for NPs preparation. Scale bar: 200 nm. (b) The chromogenic reaction shows that P4VP-CmlI NPs from microfluidic method have enzyme function fully sustained. 10 µL/min flow rate was used for the NPs sample production. 0.25 mg/mL P4VP, 1.1 mg/mL CmlI were used for co-assembly in both microfluidic method and stirring method. 1 mM pAP, 2 mM NADH, 40 µM PMS were used for the chromogenic activity assay.

between the two proteins on the NPs, which could be potentially used for bio-imaging applications [55].

4.5. Polymer-enzyme co-assembly and activity test

To further evaluate the sustained protein function on the NPs, an N-oxygenase CmlI [56] was used as a model enzyme to co-assembly with P4VP polymer by microfluidic and conventional bulk method (as reported previously) [51]. TEM image reveals highly uniform P4VP-CmlI NPs fabricated by this microfluidic method (Fig. 7a). It is worth to note that the homogeneity of P4VP-CmlI NPs is slightly better than other P4VP-proteins NPs by using microfluidic method, which could be attributed to multiple factors including protein's Mw, surface charge and hydrophobicity and others. More systematic study will be needed to understand this difference. CmlI enzyme activity can be determined by a p-nitrosophenol (pNOP) based chromogenic assay with presence of p-aminophenol (pAP) as substrate, nicotinamide adenine dinucleotide (NADH) as electron source and phenazine methosulfate (PMS) as the electron mediator (Fig. 7a inset) [51]. By comparing with the activity with the same amount of free enzyme, P4VP-CmlI NPs from either microfluidic method or bulk method show slightly higher activity than the free enzyme (Fig. 7b), which can be attributed to the faster electron transferring process upon polymer assembly. [51] This result confirms that CmlI enzyme function can be fully maintained after co-assembly with P4VP using the microfluidic system.

5. Conclusion

In this work, we described an EK-based microfluidic method to fabricate functional polymer-protein(s) NPs. The principle of fast mixing in the microchannel was illustrated qualitatively. Experimentally, we identified the size distribution of NPs fabricated by this microfluidic method could be significantly improved by comparing to that prepared by conventional bulk method due to the fast mixing process. The NPs size could be controlled by adjusting polymer/proteins ratio in the microchannel. More importantly, the functionality of proteins coated were sustained. Overall, this EK-based microfluidic method displayed great advantages to fabricate functional nanoparticles, which could be potentially used in nanoparticle preparation applications in the future.

Supplementary data to this article can be found online at https://doi.org/10.1016/j.msec.2020.110768.

CRediT authorship contribution statement

Libo Zhang: Methodology, Data curation, Formal analysis, Writing original draft. Andrew Beatty: Investigation, Writing - review & editing. Lin Lu: Investigation, Writing - review & editing. Akrm Abdalrahman: Investigation. Thomas Makris: Investigation, Funding acquisition. Guiren Wang: Project administration, Visualization,

Writing - review & editing, Supervision, Funding acquisition. **Qian Wang:** Conceptualization, Supervision, Project administration, Writing - review & editing, Funding acquisition.

Acknowledgements

This work was supported in part by the NSF and SC EPSCoR/IDeA Program under NSF Award #OIA-1655740. The views, perspective, and content do not necessarily represent the official views of the SC EPSCoR/IDeA Program nor those of the NSF. We also thank Dr. Wei Zhao for his helpful discussion and the support from the USC ASPRIE grant.

References

- [1] A.C. Balazs, T. Emrick, T.P. Russell, Science 314 (2006) 1107-1110.
- [2] J.P. Rao, K.E. Geckeler, Prog. Polym. Sci. 36 (2011) 887–913.
- [3] D.T. McQuade, A.E. Pullen, T.M. Swager, Chem. Rev. 100 (2000) 2537–2574.
- [4] L. Sha, D. Wang, Y. Mao, W. Shi, T. Gao, Q. Zhao, S. Wang, Nanotechnology 29 (2018) 345101–345122.
- [5] W.-P. Li, V. Shanmugam, C.-C. Huang, G.-D. Huang, Y.-K. Huang, S.-H. Chiu, C.-S. Yeh, Chem. Commun. (Camb.). 49 (2013) 1609–1611.
- [6] K. Hadinoto, A. Sundaresan, W.S. Cheow, Eur. J. Pharm. Biopharm. 85 (2013) 427–443.
- [7] A. Care, P.L. Bergquist, A. Sunna, Trends Biotechnol. 33 (2015) 259-268.
- [8] M. Mahmoudi, I. Lynch, M.R. Ejtehadi, M.P. Monopoli, F.B. Bombelli, S. Laurent, Chem. Rev. 111 (2011) 5610–5637.
- [9] R. Rafiei, A. Haddadi, Mater. Sci. Eng. C 104 (2019) 109950–109961.
- [10] Y. Lu, F. Xue, Z. Zhou, M. Shi, Y. Yan, L. Qin, H. Yang, S. Yang, Chemistry 20 (2014) 16242–16247.
- [11] N. Melnychuk, A.S. Klymchenko, J. Am. Chem. Soc. 140 (2018) 10856-10865.
- [12] V. Khambalkar, S. Birajdar, P. Adhyapak, S. Kulkarni, Nanotechnology 30 (2019) 105501–105515.
- [13] Y. Zhang, J. Ge, Z. Liu, ACS Catal. 5 (2015) 4503-4513.
- [14] Y. Ding, Y. Kang, X. Zhang, Chem. Commun. 51 (2014) 996–1003.
- [15] W. Fan, L. Liu, H. Zhao, Angew. Chem. Int. Ed. 56 (2017) 8844–8848.
- [16] G.A. Hudalla, T. Sun, J.Z. Gasiorowski, H. Han, Y.F. Tian, A.S. Chong, J.H. Collier, Nat. Mater. 13 (2014) 829–836.
- [17] J. Chen, M. Wu, L. Gong, J. Zhang, B. Yan, J. Liu, H. Zhang, T. Thundat, H. Zeng, J. Phys. Chem. C 123 (2019) 4540–4548.
- [18] T. Wang, X. Fan, C. Hou, J. Liu, Curr. Opin. Struct. Biol. 51 (2018) 19-27.
 - U. Unzueta, N. Serna, L. Sánchez-García, M. Roldán, A. Sánchez-Chardi, R. Mangues, A. Villaverde, E. Vázquez, Nanotechnology 28 (2017) 505102–505114.
- [20] C. Gräfe, M. von der Lühe, A. Weidner, P. Globig, J.H. Clement, S. Dutz, F.H. Schacher, Nanotechnology 30 (2019) 265707–265723.
- [21] N. Suthiwangcharoen, T. Li, L. Wu, H.B. Reno, P. Thompson, Q. Wang, Biomacromolecules 15 (2014) 948–956.
- [22] D. Tuncel, H. Volkan Demir, Nanoscale 2 (2010) 484-494.
- [23] L.A. Renna, C.J. Boyle, T.S. Gehan, D. Venkataraman, Macromolecules 48 (2015) 6353–6368.
- [24] D. Duranoğlu, D. Uzunoglu, B. Mansuroglu, T. Arasoglu, S. Derman, Nanotechnology 29 (2018) 395603–395617.
- [25] H. Zhao, Z.Y. Lin, L. Yildirimer, A. Dhinakar, X. Zhao, J. Wu, J. Mater. Chem. B 4 (2016) 4060–4071.
- [26] K. DeFrates, T. Markiewicz, P. Gallo, A. Rack, A. Weyhmiller, B. Jarmusik, X. Hu, Int. J. Mol. Sci. 19 (2018) 1717–1737.
- [27] S. Badilescu, M. Packirisamy, Polymers (4) (2012) 1278-1310.
- [28] R. Karnik, F. Gu, P. Basto, C. Cannizzaro, L. Dean, W. Kyei-Manu, R. Langer, O.C. Farokhzad, Nano Lett. 8 (2008) 2906–2912.
- [29] Y. Kim, B.L. Chung, M. Ma, W.J.M. Mulder, Z.A. Fayad, O.C. Farokhzad, R. Langer, Nano Lett. 12 (2012) 3587–3591.

- [30] D. Dendukuri, P.S. Doyle, Adv. Mater. 21 (2009) 4071-4086.
- [31] T. Li, L. Wu, N. Suthiwangcharoen, M.A. Bruckman, D. Cash, J.S. Hudson, S. Ghoshroy, Q. Wang, Chem. Commun. 20 (2009) 2869–2871.
- [32] T. Li, B. Ye, Z. Niu, P. Thompson, S. Seifert, B. Lee, Q. Wang, Chem. Mater. 21 (2009) 1046–1050.
- [33] T. Li, Z. Niu, T. Emrick, T.P. Russell, Q. Wang, Small 4 (2008) 1624-1629.
- [34] L. Lu, L. Yuan, J. Yan, C. Tang, Q. Wang, Biomacromolecules 17 (2016) 2321-2328.
- [35] Q. Feng, J. Sun, X. Jiang, Nanoscale 8 (2016) 12430-12443.
- [36] H. Kim, K.-I. Min, K. Inoue, D.J. Im, D.-P. Kim, J. Yoshida, Science 352 (2016) 691–694.
- [37] A. Dobhal, A. Kulkarni, P. Dandekar, R. Jain, J. Mater. Chem. B 5 (2017) 3404–3417.
- [38] G.R. Wang, F. Yang, W. Zhao, Lab Chip 14 (2014) 1452-1458.
- [39] G. Wang, F. Yang, W. Zhao, C.-P. Chen, Lab Chip 16 (2016) 1030-1038.
- [40] W. Zhao, F. Yang, K. Wang, J. Bai, G. Wang, Chem. Eng. Sci. 165 (2017) 113-121.
- [41] M.H. Oddy, J.G. Santiago, J.C. Mikkelsen, Anal. Chem. 73 (2001) 5822-5832.
- [42] C.-H. Chen, H. Lin, S.K. Lele, J.G. Santiago, J. Fluid Mech. 524 (2005) 263-303.
- [43] F. Yang, C. Kuang, W. Zhao, G. Wang, Chem. Eng. Commun. 204 (2017) 190-197.

- [44] W. Podgórska, D.L. Marchisio, Chem. Eng. Res. Des. 108 (2016) 30-41.
- [45] A. Ramos, H. Morgan, N.G. Green, A. Castellanos, J. Phys. Appl. Phys. 31 (1998) 2338–2353.
- [46] J.R. Melcher, Continuum Electromechanics, MIT Press, Cambridge, MA, 1981.
- [47] R.F. Probstein, Physicochemical Hydrodynamics: An Introduction, 2nd Ed, John Wiley, 2003.
- [48] J.C. Baygents, F. Baldessari, Phys. Fluids 10 (1998) 301–313.
- [49] G.A. Truskery, F. Yuan, D.F. Katz, Transport Phenomena in Biological Systems, 2nd ed., Person, Prentice Hall, 2010.
- [50] J. Ma, S.M.-Y. Lee, C. Yi, C.-W. Li, Lab Chip 17 (2017) 209-226.
- [51] L. Zhang, Y. Xu, T.M. Makris, Q. Wang, Biomacromolecules 19 (2018) 918-925.
- [52] L. Lu, L. Zhang, L. Yuan, T. Zhu, W. Chen, G. Wang, Q. Wang, ChemBioChem (2019) 1394–1399.
- [53] B.J. Kirby, Micro- and Nanoscale Fluid Mechanics: Transport in Microfluidic Devices, Cambridge University Press, NY, 2010.
- [54] B.K. Johnson, R.K. Prud'homme, Phys. Rev. Lett. 91 (2003) 118302-118306.
- [55] Y. Arai, T. Nagai, Microscopy (Oxf) 62 (2013) 419-428.
- [56] H. Lu, E. Chanco, H. Zhao, Tetrahedron 68 (2012) 7651-7654.